



Supercritical carbon dioxide-assisted gold metallization of 3D-printed structure and the tensile strength

Po-Wei Cheng, Tomoyuki Kurioka, Chun-Yi Chen , Tso-Fu Mark Chang, Wan-Ting Chiu, and Hideki Hosoda, Institute of Innovative Research, Tokyo Institute of Technology, Yokohama, Kanagawa 226-8503, Japan

Kei Takase, Diagnostic Radiology, Tohoku University Graduate School of Medicine, Sendai 980-8575, Japan

Hiroshi Ishihata, Division of Periodontology and Endodontology, Department of Ecological Dentistry, Tohoku University Graduate School of Dentistry, Sendai 980-8575, Japan

Masato Sone, Institute of Innovative Research, Tokyo Institute of Technology, Yokohama, Kanagawa 226-8503, Japan

Address all correspondence to Chun-Yi Chen at chen.c.ac@m.titech.ac.jp

(Received 23 January 2023; accepted 17 May 2023; published online: 30 May 2023)

Abstract

Gold metallization of 3D printed polymer structures was conducted by a supercritical carbon dioxide (sc-CO₂) assisted electroless plating process. Precursor of the Pd catalyst utilized in this study was palladium bis-hexafluoroacetylacetonate for the high solubility in sc-CO₂. A Ni–P layer was first formed on the catalyzed polymer structure as a sacrificial layer for the sequential gold deposition. Electrical resistance of the gold metallized 3D printed structure was 0.15 Ω and slightly increased to 0.18 Ω after a tape adhesion test. The fracture strength was 47.6 MPa for the sample with 45 min of the gold deposition time.

Introduction

Additive manufacturing also known as three-dimensional (3D) printing technology is a process adopted to create 3D modules from digital designs. In the last decade, it has attracted great attention due to its high degree of freedom and precise resolution on complex 3D structure design. Selections of the ink material and fabrication duration are considered to be primary focus in this research field.^[1] Recently, the interests of 3D printing technology have been extended to fabrication of various functional electronic components,^[2] electromagnetics,^[3] wearable devices,^[4] and bio-engineering.^[5] For applications of 3D printed polymer structures in aforementioned technologies, metallization is essential and could be realized by approaches of physical^[6] and chemical vapor deposition,^[7] sputtering,^[8] and electroless plating.^[9–14]

Electroless plating is considered to be the most ideal process among the metallization approaches due to its great capability to deposit metal coatings on complex structures and facile properties manipulating on the deposited metal coating.^[15–17] There are three core steps in electroless plating, which are pretreatment step, catalyzation step, and metal deposition step. First, surfaces of the insulating substrate are cleaned and roughed to elevate interactions between the processed substrate and later-decorated catalyst seeds. Second, catalyst seeds are decorated on the substrate surface in the catalyzation step. Last, deposition process of metals is activated at the catalyst seeds to gradually cover the entire substrate surface in the deposition step.

In the pretreatment step, roughened substrate surface is acquired by using an etching solution, which is not an environmentally friendly approach due to the etching solution's toxicity. Also, in the conventional catalyzation step, only a

limited amount of the catalyst seeds is remained on surfaces of the substrate, and this is a critical factor affecting interaction between the deposited metal coating and the substrate. Therefore, a catalyzation process utilizing supercritical carbon dioxide (sc-CO₂) as the solvent is proposed for metallization of polymer materials.^[14, 18, 19] CO₂ is inexpensive, non-toxic and non-polar, and it possesses high self-diffusivity and zero surface tension^[20] when it reaches its critical point (7.4 MPa and 31°C).^[21, 22] These are all beneficial for transferring materials into non-polar polymer structures to improve interactions between the metal coating and the substrate. In sc-CO₂ catalyzation, organometallic compounds dissolved in sc-CO₂ could be transferred into the polymer substrate to allow formation of catalyst seeds inside the polymer structure.^[23] Then, metals would form from the catalyst seeds inside the polymer substrate to promote interactions between the metal layer and the polymers. Additionally, by the sc-CO₂ catalyzation step, the pretreatment step is no longer required, and this implies usage of environmentally unfriendly solvents could be prevented.

In a previous study, Ni–P metallization of 3D printed polymers is realized by the sc-CO₂-assisted electroless plating.^[14] The electrical resistance of Ni–P metallized 3D-printed square pad is 0.03 Ω, and the electrical resistance merely increases to 0.04 Ω after a tape adhesion test. Regarding the metal layer, chemical stability and biocompatibility of gold are all better than those of Ni–P. Most importantly, the difference in the ductility between gold and 3D printed polymers is smaller than that between Ni–P and 3D printed polymers. These all make gold a promising material to be integrated with 3D printed polymers toward additive manufacturing of electronic components.

In this study, gold metallization of 3D printed polymers is conducted by the *sc*-CO₂-assisted electroless plating process. Palladium bis-hexafluoroacetylacetonate (Pd(hfa)₂), an organometallic compound, is chosen as a source of the catalyst for its high solubility in *sc*-CO₂. The solubility of Pd(hfa)₂ in *sc*-CO₂ is greater than 3.6 wt% (or 3.15×10^{-3} mol fraction) at 8.9 MPa and 313.2 K.^[24] The reliability of gold metallized 3D printed polymer is evaluated by tape adhesion test and tensile test.

Experimental

3D printing

The 3D printer (MARS 2 PRO MONO LCD MSLA resin 3D printer) and photopolymer resin (Standard LCD UV-Curing Photopolymer Rapid Resin for 3D Printers) were purchased from Elegoo Inc. The resin was composed of phenolic epoxy resin (40–50 wt%), 6-hexanediol diacrylate (20–40 wt%), color pigment (2–5%), and 1-hydroxycyclohexyl phenyl ketone (3–5 wt%). UV light at $\lambda = 405$ nm was used as the light source in photopolymerization of the resin. For the tensile test, a dog-bone shaped structure was prepared. A schematic diagram of the dog-bone shaped structure is provided in Fig. 1(a).

Catalyzation

A commercial catalyzation solution (Okuno Chemical Industries Co., Ltd.: ICP Accera KCR) was used to catalyze the 3D printed polymer structures to be used as comparison treated by the *sc*-CO₂ catalyzation. For the conventional catalyzation step (CONV), the experimental conditions were 30°C and 30 min. For the *sc*-CO₂ catalyzation step, the *sc*-CO₂ equipment was provided by Japan Spectra Company. The reaction cell was constructed by stainless steel 316 with polyether ether ketone coating on the inner wall, and the inner volume was 50.0 ml. More details of the *sc*-CO₂ equipment were addressed in a previous study.^[18] The 3D printed polymer structure and 50 mg

of palladium bis-hexafluoroacetylacetonate (Pd(hfa)₂, Sigma-Aldrich) were placed in the reaction cell. After sealing the reaction cell properly, liquidized CO₂ was pumped into the reaction. The pressure was controlled at 15 MPa, and the temperature was at 70.0°C. The catalyzation time was 1.0 h.

Metal deposition

After the catalyzation step, the catalyzed 3D printed polymer structures were immersed into a Ni–P electroless plating solution (Okuno Chemical Industries Co., Ltd: Top Nicoron VS-LF) for 3.0 min at 70.0°C. The Ni–P plating solution is composed of nickel chloride (9 wt%), sodium hypophosphite (12 wt%), complexing agent (12 wt%), and ion-exchanged water (67 wt%). In electroless plating of gold,^[18] decoration of less noble metals on the catalyzed substrate is required to be used as the sacrificial material before deposition of gold. And, Ni–P was chosen as the sacrificial material in this study. In addition, a sensitization step by immersing the Ni–P decorated 3D printed polymer structures in a 0.1 mM KAuCl₄ (99.995%, Sigma-Aldrich) solution for 1 h at 30.0°C was conducted. Then the Ni–P decorated/KAuCl₄ sensitized/3D printed polymer structures were placed in a commercially available gold electroless plating solution (MATEX Japan Co., Ltd.: Non-Cyanide Electroless Solution, and the solution contained 2 g/L of Au with pH at 7) for 15.0 min, 30.0 min and 45.0 min at 65°C to cover the entire surface with gold.

Characterization

Surface morphologies and cross-section of the gold metallized 3D printed polymer structures were observed by a scanning electron microscope (SEM, HITACHI: S-4300SE). The thickness of the gold layer was determined through observing the cross-section, and the thickness of at least five locations was obtained and averaged to be used as the reported thickness. Crystal structures and phase of the gold metallized 3D printed

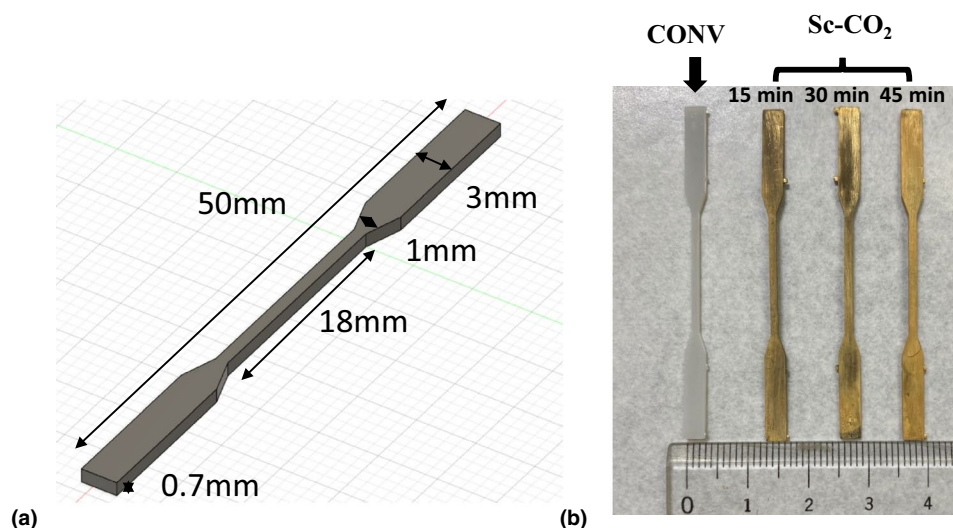


Figure 1. (a) A schematic design of the 3D printed dog-bone structure and (b) images of the 3D printed dog-bone structures after the gold deposition step.

polymer structures were identified by X-ray diffraction (XRD, Rigaku: Ultima IV). The electrical resistance was examined by a four-point probe (Mitsubishi Chemical Analytech Co., Ltd.: MCP-T37). Intactness of the gold layer on the 3D printed polymer structures was investigated by a tape adhesion test.^[14, 18] The tape adhesion test was conducted by firmly sticking a piece of 3 M Scotch® tape onto the gold metallized sample surface with a 1 kg load. After removing the load and peeling the tape off the sample surface in sequence, the electrical resistance was measured again. The tape adhesion test was conducted three times using different samples prepared under same conditions to provide a reliable result. The tensile test was conducted by a universal testing machine (Shimadzu Corp.: Autograph Instron–type AG-500NI). The electrical resistance of the dog-bone shaped structure was monitored by an electrical resistance meter (HIOKI E.E. CORPORATION.: RM3544) during the tensile test to determine the fracture point. Also, a video (Canon: HFR32) was taken during the tensile test.

Results and discussion

Surface appearances of the 3D printed dog-bone shaped structures after the gold deposition step are provided in Fig. 1(b). The original color of the photopolymer resin is grey. The conventional catalyzed sample remained the color of the photopolymer resin after the gold deposition step, and this revealed unsuccessful metallization of the 3D printed polymer structures. On the other hand, the gold metallization was successful for the sc-CO₂ catalyzed samples, which showed

metal-like golden color after the gold deposition step. The results suggested the conventional catalyzed sample was ineffective in decoration of Pd catalyst seeds on the 3D printed polymer structure, hence, the gold deposition was not possible for the conventional catalyzed sample.

X-ray diffraction patterns of the as-printed polymer structure is provided in Fig. 2(a). Signals at around $2\theta=20^\circ$ were contributed by the solidified photopolymer resin. After decoration of Ni–P on the sc-CO₂ catalyzed sample [Fig. 2(b)], a broad peak at signals at around $2\theta=45^\circ$ was observed, and this suggested presence of amorphous Ni–P, which is commonly acquired in Ni–P obtained by electroless plating.^[25] After the gold deposition, the XRD patterns are shown in Fig. 2(c) to (e). Signals at around $2\theta=40^\circ, 45^\circ, 65^\circ, 78^\circ$ and 83° could be assigned to face-centered cubic (FCC) crystal structure of gold (JCPDS card No 46-1043). In Fig. 2(c), contributions from the photopolymer resin were obvious, and the two FCC gold peaks at $2\theta=40^\circ$ and 45° were not that sharp, which is suggested to be influenced by the amorphous Ni–P, in the 15.0 min gold metallized sample. As the gold deposition time increased to 30.0 min and 45.0 min, relative intensities of the photopolymer resin gradually decreased, and influences of the amorphous Ni–P became less observable. These findings suggested an increasing trend of the amount of gold deposited on the sample.

Surface conditions of the gold metallized samples were evaluated from the SEM images shown in Fig. 3(a) to (c). In Fig. 3(a), surfaces of the 15.0 min sample were covered with many tiny particles, and these particles were believed to be gold. Some portion of the surface showed a darker color

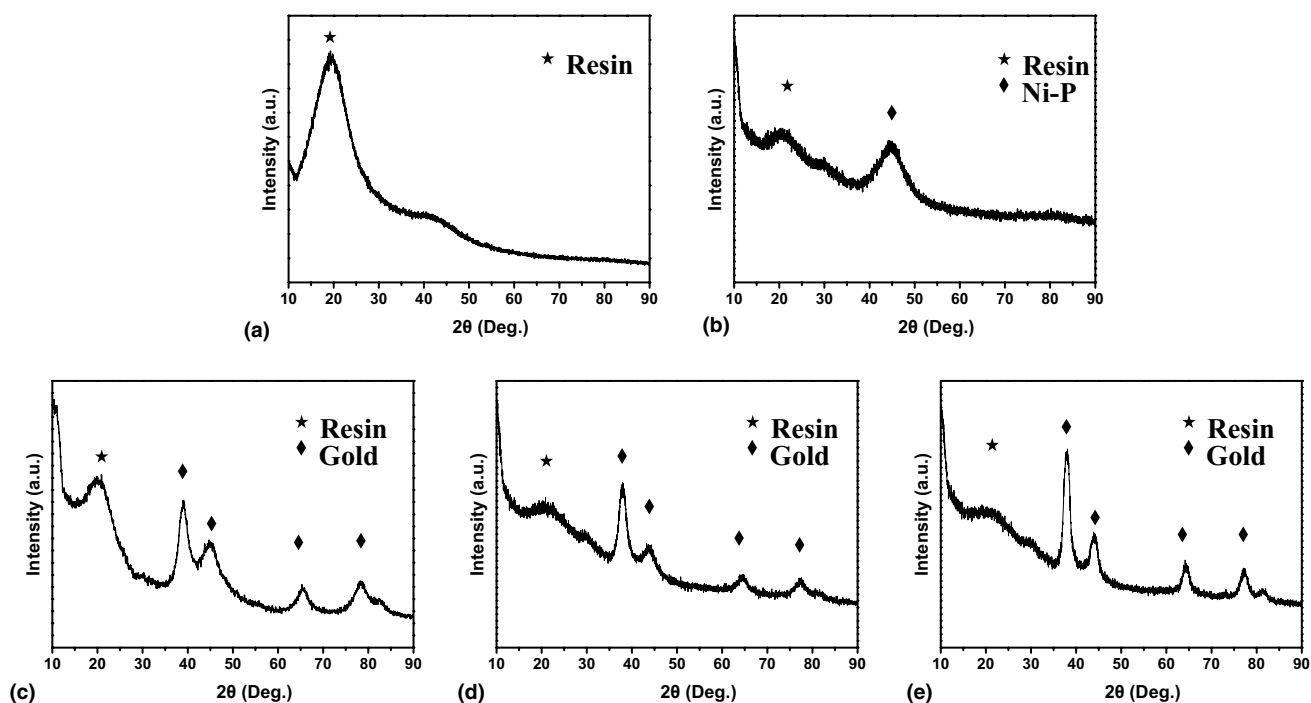


Figure 2. XRD of (a) 3D printed polymer structure, (b) Ni–P decorated and sc-CO₂ catalyzed sample, and gold metallized 3D printed polymer structure with (c) 15.0 min, (d) 30.0 min and (e) 45.0 min of the gold deposition time.

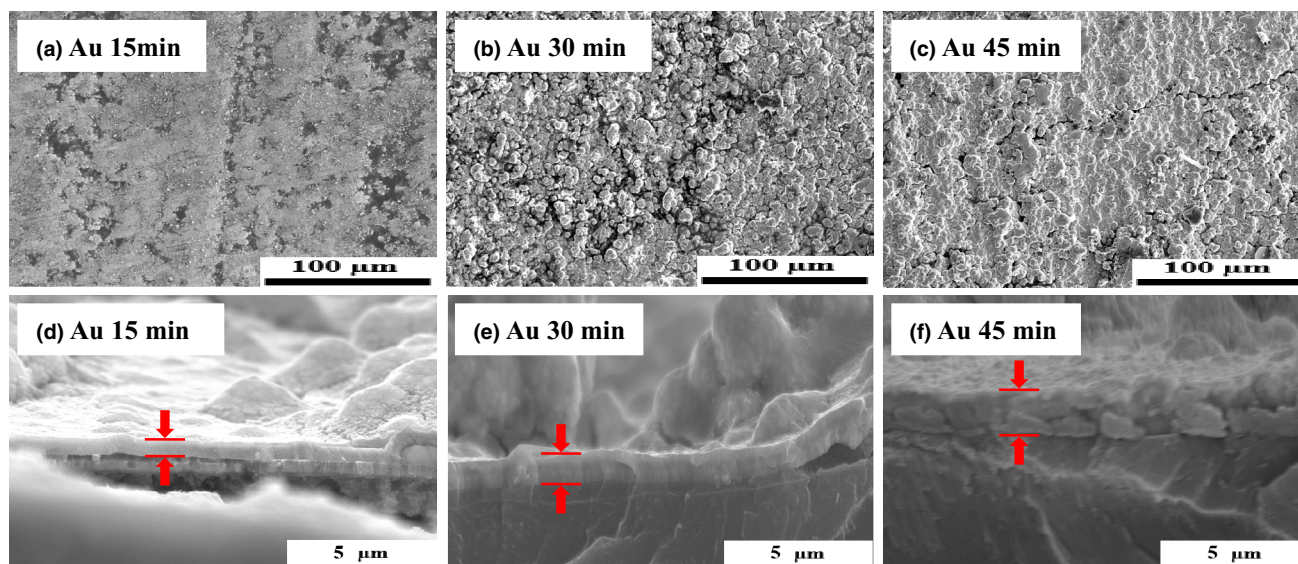


Figure 3. Surface conditions of the gold metallized 3D printed polymer structures prepared with (a) 15.0 min, (b) 30.0 min and (c) 45.0 min of the gold deposition time, and cross-sectional view of the samples with (d) 15.0 min, (e) 30.0 min, and (f) 45.0 min of the gold deposition.

than the color of the tiny particles, and this was suggested to be regions still not covered with gold. As the gold deposition time increased to 30.0 min, sizes of the particles increased, and the entire surface was covered with the particles as shown in Fig. 3(b). In Fig. 3(c), the average size of the particles did not change much, but boundaries of the particles became less obvious as the gold deposition time extended to 45.0 min.

Examples of the cross-sectional images used to determine the gold layer thickness are provided in Fig. 3(d) to (f). The gold layer thickness reached $0.48 \pm 0.11 \mu\text{m}$ after 15.0 min of the gold deposition time, and it thickened to $0.92 \pm 0.12 \mu\text{m}$ and $1.23 \pm 0.26 \mu\text{m}$ as the gold deposition time prolonged to 30.0 min and 45.0 min, respectively. An increase in the gold layer thickness corresponded well with the relative XRD signal intensity [Fig. 2(c) to (e)] and surface condition [Fig. 3(a) to (c)] results, which the amount of gold on the sample increased following an increase in the gold deposition time. The relationships between the gold deposition time, gold layer thickness and gold growth rate were plotted and shown in Fig. 4(a). The gold

growth rate in the first 15.0 min interval of the gold deposition time was calculated to be $0.032 \mu\text{m}/\text{min}$, and the gold growth rate gradually decreased to $0.029 \mu\text{m}/\text{min}$ and $0.021 \mu\text{m}/\text{min}$ for the second and third 15.0 min interval, respectively, of the gold deposition time. Reduction of the gold growth rate was suggested to be a result of a decrease in the concentration of reactive species in the gold electroless plating solution.

The electrical resistance of the 15.0 min sample was 0.70Ω , and it reduced to 0.28Ω and 0.15Ω , indicating an improved electrical conductivity, as the gold deposition time extended to 30.0 min and 45.0 min, respectively. After the tape adhesion test, the electrical resistances slightly increased to 0.83Ω , 0.35Ω and 0.18Ω for the 15.0 min, 30.0 min and 45.0 min samples, respectively. The results are summarized in Fig. 4(b). The conductive properties are tabulated in Table S1. Generally, the electrical resistance remained at a low level after the tape adhesion test, and this demonstrated the strong interaction between the gold layer and the 3D printed structure by the sc- CO_2 catalysis in metallization of 3D printed polymer structures.

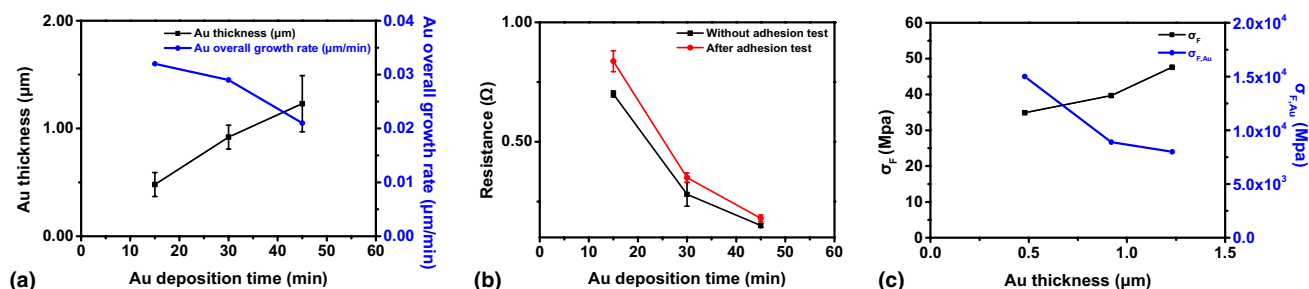


Figure 4. Plots of (a) the gold deposition time versus the gold layer thickness and gold growth rate, (b) the gold deposition time versus the electrical resistance, and (c) the gold layer thickness versus the two fracture strengths (σ_F and $\sigma_{F,Au}$).

The fracture strength (σ_F) of the as-printed dog-bone shaped structure was 23.0 MPa. After the gold metallization, the fracture strength increased to 34.9 MPa for the 15.0 min sample, and the fracture strength reached 39.7 MPa and 47.6 MPa as the gold deposition time increased to 30.0 min and 45 min, respectively. The engineering stress-engineering strain curves for each sample are provided in Fig. S1. A video showing the tensile test and the engineering stress-engineering strain curves used to determine the fracture strength is provided as a supplementary video. Figure 4(c) shows the relationship between the gold layer thickness and the fracture strength. In general, strengthening of the 3D printed structure was obtained by depositing more gold on the sample. The fracture strength of pure gold is 120 MPa,^[26] which is much larger than the fracture strength than the as-printed dog-bone shaped structure. Therefore, it was expected to see an increase in the fracture strength after the gold metallization.

In a further analysis on the contribution of the metallized gold to the fracture strength, a value of the fracture force divided by the area of the metallized gold in the cross-section ($\sigma_{F,Au}$) was calculated as indicated in the following equation:

$$\sigma_{F,Au} = \frac{\text{The force when fracture occurs}}{\text{Cross - sectional area of the gold in the sample}}$$

A plot of the gold layer thickness versus the $\sigma_{F,Au}$ is provided in Fig. 4(c). A decreasing trend was observed following an increase in the amount of gold metallized onto the 3D printed structure. In mechanical characterization of small-sized metal-based materials, the mechanical strength is reported to be dependent on the size of the sample used in the mechanical test, which is known as the sample size effect.^[27] Usually, a smaller-is-stronger is reported when reducing the sample size from bulk-size to micro-scale or smaller. The higher $\sigma_{F,Au}$ obtained as the gold layer thickness decreased is to some extent similar to the smaller-is-stronger phenomenon in the sample size effect.

Conclusion

Additive manufacturing of gold metallized 3D structures was demonstrated in this study. Complete gold metallization of the 3D printed structures was realized by sc-CO₂-assisted electroless plating. The sc-CO₂ was employed as a solvent to promote interaction between the Pd catalyst and surfaces of the 3D printed structures in the catalyzation step, and this eventually contributed to the complete gold metallization. Thickness of the gold layer reached 0.48 μm after 15.0 min of the gold deposition time, and the thickness was elevated to 1.23 μm as the gold deposition time increased to 45.0 min. The electrical resistance showed a negative correlation with the gold deposition time. The sample with 15.0 min of the gold deposition time showed the electrical resistance at 0.70 Ω , and it was reduced to 0.15 Ω when the gold deposition time was extended to 45.0 min. For the 45.0 min sample, the electrical resistance slightly worsened to 0.18 Ω . In addition, the strengthening was observed in the gold metallized samples, and the highest fracture strength was 47.6 MPa for the 45.0 min sample. In conclusion, the gold

metallized 3D printed structures reported in this study are promising materials toward electronic components by the low electrical resistance, resistant again the tape adhesion test, and promoted tensile fracture strength.

Acknowledgments

This research is supported by the JSPS KAKENHI Grant Number JP21H01668 and JP21H00807, and based on the Cooperative Research Project of Research Center for Biomedical Engineering.

Data availability

The data that support the findings of this study are available from the corresponding author upon reasonable request.

Declarations

Conflict of interest

On behalf of all of the co-authors, the corresponding author states that there is no conflict of interest.

Open Access

This article is licensed under a Creative Commons Attribution 4.0 International License, which permits use, sharing, adaptation, distribution and reproduction in any medium or format, as long as you give appropriate credit to the original author(s) and the source, provide a link to the Creative Commons licence, and indicate if changes were made. The images or other third party material in this article are included in the article's Creative Commons licence, unless indicated otherwise in a credit line to the material. If material is not included in the article's Creative Commons licence and your intended use is not permitted by statutory regulation or exceeds the permitted use, you will need to obtain permission directly from the copyright holder. To view a copy of this licence, visit <http://creativecommons.org/licenses/by/4.0/>.

Supplementary Information

The online version contains supplementary material available at <https://doi.org/10.1557/s43579-023-00373-y>.

References

1. D. Ahn, L.M. Stevens, K. Zhou, Z.A. Page, ACS Cent. Sci. **6**, 1555 (2020). <https://doi.org/10.1021/acscentsci.0c00929>
2. N.A. Shepelin, V.C. Lussini, P.J. Fox, G.W. Dicoski, A.M. Glushenkov, J.G. Shapter, A.V. Ellis, MRS Commun. **9**, 159 (2019). <https://doi.org/10.1557/MRC.2019.19>
3. J. Bito, R. Bahr, J.G. Hester, S.A. Nauroze, A. Georgiadis, M.M. Tentzeris, IEEE Trans. Microw. Theory Tech. **65**, 1831 (2017). <https://doi.org/10.1109/TMTT.2017.2660487>
4. K. Liang, S. Carmone, D. Brambilla, J.C. Leroux, Sci. Adv. **4**, 5 (2018). <https://doi.org/10.1126/sciadv.aat2544>

5. J.R.H. Joseph-Rey, Q. Chen, R.D. Maalihan, J. Ren, Í.G.M. da Silva, N.P. Dugos, E.B. Caldoná, R.C. Advincula, *MRS Commun.* **11**, 197 (2021). <https://doi.org/10.1557/S43579-021-00038-8>
6. A. Romani, A. Mantelli, P. Tralli, S. Turri, S. Turri, M. Levi, R. Suriano, *Technology* **9**, 49 (2021). <https://doi.org/10.3390/technologies9030049>
7. M.H. Tsai, S.C. Sun, H.T. Chiu, S.H. Chuang, *Appl. Phys. Lett.* **68**, 1412 (1998). <https://doi.org/10.1063/1.116097>
8. A. Redondo-Cubero, F.J. Palomares, K. Lorenz, J. Rubio-Zuazo, R. Hübner, F.J. Mompeán, M. García-Hernández, G.R. Castro, L. Vázquez, *Appl. Surf. Sci.* **580**, 152267 (2022). <https://doi.org/10.1016/J.APSUSC.2021.152267>
9. T. Furuhashi, Y. Yamada, M. Hayashi, S. Ichihara, H. Usui, *MRS Commun.* **7**, 953 (2017). <https://doi.org/10.1557/MRC.2017.124>
10. T. Furuhashi, Y. Yamada, M. Hayashi, S. Ichihara, H. Usui, *MRS Commun.* **9**, 352 (2019). <https://doi.org/10.1557/MRC.2018.239>
11. X. Yu, Y. Hou, X. Ren, C. Sun, M. Wang, *J. Water Process Eng.* **46**, 102577 (2022). <https://doi.org/10.1016/J.JWPE.2022.102577>
12. C. Fu, S. Weng, J. Fan, Y. Zhang, Y. Guo, W. Hao, *Chem. Eng. J.* **430**, 132881 (2022). <https://doi.org/10.1016/J.CEJ.2021.132881>
13. C. Gui, R. Zhang, Z. Chen, W. Wu, H. Li, J. Huang, *Compos. Sci. Technol.* **218**, 109187 (2022). <https://doi.org/10.1016/J.COMPSCITECH.2021.109187>
14. P.W. Cheng, C.Y. Chen, T. Ichibayashi, T.F.M. Chang, M. Sone, S. Nishimura, *MRS Commun.* **11**, 278 (2021). <https://doi.org/10.1557/S43579-021-00022-2>
15. M. Shimizu, Y. Tsushima, S. Arai, *ACS Omega* **2**, 4306 (2017). <https://doi.org/10.1021/acsomega.7b00950>
16. J.M. Li, C.C. Hu, T.H. Wu, Y.J. Hsu, *RSC Adv.* **9**, 4239 (2019). <https://doi.org/10.1039/C8RA07810F>
17. T. Homma, A. Tamaki, H. Nakai, T. Osaka, *J. Electroanal. Chem.* **599**, 131 (2003). [https://doi.org/10.1016/S0022-0728\(03\)00042-1](https://doi.org/10.1016/S0022-0728(03)00042-1)
18. P.W. Cheng, C.Y. Chen, T. Ichibayashi, T.F.M. Chang, M. Sone, S. Nishimura, *J. Supercrit. Fluids* **180**, 105455 (2022). <https://doi.org/10.1016/J.SUPFLU.2021.105455>
19. M. Mitsumoto, C.Y. Chen, W.T. Chiu, T.F.M. Chang, Y. Watanabe, A. Jinno, H. Kurosu, M. Sone, *Micro Nano Eng.* **15**, 100132 (2022). <https://doi.org/10.1016/J.MNE.2022.100132>
20. H. Higashi, Y. Iwai, Y. Arai, *Chem. Eng. Sci.* **56**, 3027 (2001). [https://doi.org/10.1016/S0009-2509\(01\)00003-3](https://doi.org/10.1016/S0009-2509(01)00003-3)
21. W. Leitner, *Acc. Chem. Res.* **35**, 746 (2002). <https://doi.org/10.1021/ar010707q>
22. D. Dhamodharan, C.W. Park, P.N.P. Ghoderao, H.S. Byun, *J. Ind. Eng. Chem.* **110**, 367 (2022). <https://doi.org/10.1016/J.JIEC.2022.03.013>
23. H. Adachi, K. Taki, S. Nagamine, A. Yusa, M. Oshima, *J. Supercrit. Fluids* **49**, 265 (2009). <https://doi.org/10.1016/j.supflu.2008.12.010>
24. M.J. Tenorio, A. Cabañas, C. Pando, J.A.R. Renuncio, *J. Supercrit. Fluids* **70**, 106 (2012). <https://doi.org/10.1016/J.SUPFLU.2012.06.014>
25. J.Y. Song, J. Yu, *Thin Solid Films* **415**, 167 (1984). [https://doi.org/10.1016/S0040-6090\(02\)00556-4](https://doi.org/10.1016/S0040-6090(02)00556-4)
26. S.B. Son, H. Roh, S.H. Kang, H.S. Chung, D.H. Kim, Y.S. Choi, J.S. Cho, J.T. Moon, K.H. Oh, *Gold Bull.* **44**, 231 (2011). <https://doi.org/10.1016/J.MEE.2020.111233>
27. A.T. Jennings, M.J. Burek, J.R. Greer, *Microstructure versus Size: Mechanical properties of electroplated single crystalline Cu nanopillars.* *Phys. Rev. Lett.* **104**, 135503 (2010). <https://doi.org/10.1103/PhysRevLett.104.135503>

Publisher's Note Springer Nature remains neutral with regard to jurisdictional claims in published maps and institutional affiliations.